

This is the accepted manuscript made available via CHORUS. The article has been published as:

## How massless neutrinos affect the cosmic microwave background damping tail

Zhen Hou, Ryan Keisler, Lloyd Knox, Marius Millea, and Christian Reichardt

Phys. Rev. D **87**, 083008 — Published 23 April 2013

DOI: [10.1103/PhysRevD.87.083008](https://doi.org/10.1103/PhysRevD.87.083008)

# How Massless Neutrinos Affect the Cosmic Microwave Background Damping Tail

Zhen Hou<sup>1</sup>, Ryan Keisler<sup>2</sup>, Lloyd Knox<sup>1</sup>, Marius Millea<sup>1</sup> and Christian Reichardt<sup>3</sup>

<sup>1</sup>*Department of Physics, One Shields Avenue, University of California, Davis, California 95616, USA;* <sup>2</sup>*Department of Astronomy & Astrophysics, University of Chicago, 5640 S. Ellis Avenue, Chicago, Illinois 60637, USA;* <sup>3</sup>*Department of Physics, University of California, Berkeley, CA 94720, USA;*

We explore the physical origin and robustness of constraints on the energy density in relativistic species prior to and during recombination, often expressed as constraints on an effective number of neutrino species,  $N_{\text{eff}}$ . If the primordial Helium abundance,  $Y_{\text{P}}$ , follows the prediction of Big-Bang nucleosynthesis (BBN) theory, the constraint on  $N_{\text{eff}}$  from current CMB anisotropy data is almost entirely due to the impact of the neutrinos on the expansion rate, and how those changes to the expansion rate alter the ratio of the photon diffusion scale to the sound horizon scale at recombination. We demonstrate that, as long as the primordial helium abundance is derived in a BBN-consistent manner, the constraint on  $N_{\text{eff}}$  degrades little after marginalizing over  $A_{\text{eISW}}$ , the phenomenological parameter characterizing the amplitude of the early Integrated Sachs-Wolfe (ISW) effect. We also provide a first determination of  $A_{\text{eISW}}$ . Varying the  $Y_{\text{P}}$ , also changes the ratio of damping to sound-horizon scales. We study the physical effects that prevent the resulting near-degeneracy between  $N_{\text{eff}}$  and  $Y_{\text{P}}$  from being a complete one and find the early ISW effect does play a role in breaking this degeneracy. Examining light element abundance measurements, we see no significant evidence for evolution of  $N_{\text{eff}}$  and the baryon-to-photon ratio from the epoch of BBN to decoupling. Finally, we consider measurements of the distance-redshift relation at low to intermediate redshifts and their implications for the value of  $N_{\text{eff}}$ .

## I. INTRODUCTION

High-resolution observations of the cosmic microwave background (CMB) temperature anisotropy are providing a precise measurement of the damping tail of CMB power spectrum, shedding light on the physical conditions during recombination and back into the radiation dominated era. The measurements have revealed somewhat less fluctuation power at small angular scales than expected in the standard cosmological model [1–4]. Many papers [3–9] have considered the possibility that this deficit of power is due to extra (dark) relativistic species [54], such as nearly massless sterile neutrinos. Constraints are usually expressed in terms of an effective number of neutrinos,  $N_{\text{eff}}$  [55].

Note that these constraints apply to any weakly interacting or non-interacting species that is relativistic at recombination. Hypothesized additional species include sterile neutrinos, sub-eV mass axions as in, e.g., Hannestad et al. [10] and those arising in many other extensions of the standard model such as in Fischler and Garcia [11].

Interest in the number of light degrees of freedom is further stimulated by i) recent inferences of the primordial Helium abundance which are larger, and with larger uncertainties than previous analyses [12–14], ii) evidence for additional (sterile) neutrino species from laboratory-produced neutrinos [15] and reactor-produced neutrinos [16] and iii) a slight tension between determinations of distance vs. redshift at very low redshifts (essentially measurements of  $H_0$  [17]) and those at low to intermediate redshifts that use the baryon acoustic oscillation (BAO) feature in the galaxy power spectrum as a CMB-calibrated standard ruler [18, 19].

Given this interest, and impending improvements to the damping tail measurements from the SPT [4] (K11

hereafter) and the *Planck* satellite, a pedagogical exposition of the impact of  $N_{\text{eff}}$  on the CMB is quite timely. The relevant physics is beautifully simple and deserves to be as well (and as broadly) understood as the constraints on  $N_{\text{eff}}$  from BBN considerations. Focusing on the physics behind the constraints also allows one to understand their more general implications. The only important assumptions about the relativistic degrees of freedom that go into the CMB predictions is that their interactions are negligible and they are massless.

Despite the analyses provided by Hu and White [20] and Bashinsky and Seljak [21] we find that the mechanism for constraining  $N_{\text{eff}}$  is not broadly understood, and in some cases misunderstood. The sensitivity to  $N_{\text{eff}}$  from high-resolution CMB observations is due to the impact of the mean relativistic energy density on the Universe’s expansion rate prior to (and during) the epoch of photon-baryon decoupling. As we demonstrate below, neutrino perturbations do not play a significant role [56], nor do anisotropies induced after decoupling. To study how much the early ISW effect plays a role in the estimation of  $N_{\text{eff}}$ , we introduce a phenomenological scaling of its physical value by a parameter  $A_{\text{eISW}}$  and examine the constraints on  $N_{\text{eff}}$  that follow from marginalizing over  $A_{\text{eISW}}$ .

The constraints on  $N_{\text{eff}}$  are model dependent; there are other ways to extend the standard cosmological model to suppress small-scale power in the cosmic microwave background. We discuss, in particular, departures from a power law for the primordial perturbation spectrum, and allowing the fraction of baryonic mass in Helium,  $Y_{\text{P}}$ , to be a free parameter.

We also consider the sensitivity of inferences of  $N_{\text{eff}}$  from CMB data to assumptions about BBN and measurements of light-element abundances. Allowing  $Y_{\text{P}}$  to vary

freely introduces a degeneracy that completely changes the mechanism by which  $N_{\text{eff}}$  is constrained by CMB data. We comment on the origin of constraints in the  $N_{\text{eff}} - Y_{\text{P}}$  plane.

In Section II we review the analytic explanation for the origin of constraints on  $N_{\text{eff}}$  from CMB observations and demonstrate its quantitative effectiveness in understanding constraints from current data. We also examine the model dependence of constraints on  $N_{\text{eff}}$ . In Section III we consider the impact of the early ISW effect on  $N_{\text{eff}}$  constraints and we discuss our results and conclude in Section IV.

## II. HOW CMB OBSERVATIONS CONSTRAIN COMPONENT DENSITIES

Let us review the sensitivity of the CMB power spectrum to the densities today of baryons,  $\rho_b$ , cold dark matter plus baryons,  $\rho_m$ , and the dark energy,  $\rho_\Lambda$ , all within the context of the  $\Lambda$ CDM model [57]. For more details than we give here, see [22, 23]. In the course of our review, we will identify directions in parameter space that cause large changes in probability density. When we do study variations in  $N_{\text{eff}}$  we will do so along orthogonal directions.

### A. Sensitivity to the Non-neutrino Components

The dependence of the CMB on  $\rho_b$  arises from the dependence of the equation-of-state of the pre-recombination plasma on the fraction of its energy density that comes from baryons. Increasing the number of baryons per photon decreases the plasma's pressure to density ratio ( $P/\rho$ ). The resulting shift in the equilibrium point between gravitational and pressure forces alters the ratio of even peak heights to odd peak heights. We know the energy density of photons very well from measuring the CMB photon spectrum [24], and can thus infer  $\rho_b$  from the ratio of even to odd peak heights.

The dependence on  $\rho_m$  arises from the sensitivity of the evolution of a Fourier mode amplitude to the fraction of the energy density contributed by non-relativistic matter when the mode's wavelength is equal to the Hubble radius. This ratio depends on  $\lambda/r_{\text{EQ}}$  where  $\lambda$  is the comoving wavelength,  $r_{\text{EQ}} = H_{\text{EQ}}^{-1}/a_{\text{EQ}}$  defines the comoving Hubble radius at the time when the matter density equals the radiation density (an epoch denoted by 'EQ') and  $a$  is the scale factor parameterizing the expansion of the Universe. The amplitude of a mode projecting to angular scale  $\theta$  depends on  $\theta/\theta_{\text{EQ}}$  where  $\theta_{\text{EQ}} = r_{\text{EQ}}/D_A$  because  $\theta/\theta_{\text{EQ}} = \lambda/r_{\text{EQ}}$ . Since the amplitude is a strong function of this ratio, there is strong sensitivity to  $\theta_{\text{EQ}}$  and therefore to  $z_{\text{EQ}}$  ( $1+z = 1/a$ ) since, assuming the dark energy is a cosmological constant,  $\theta_{\text{EQ}} = I(\Omega_m)/\sqrt{1+z_{\text{EQ}}}$  where  $I(\Omega_m)$  is a very slowly-varying function of  $\Omega_m$  [58].

Thus the CMB power spectrum is sensitive to  $1+z_{\text{EQ}} = \rho_m/\rho_r$ . If we *assume* the standard radiation content ( $N_{\text{eff}} = 3.046$ ,  $\rho_r = \rho_\gamma + \rho_\nu$ ), then a constraint on  $1+z_{\text{EQ}}$  directly constrains  $\rho_m$ . However, if we are allowing  $N_{\text{eff}}$  to vary, we should study its effects at fixed  $1+z_{\text{EQ}}$  since this quantity is well constrained by the data. Prior to the CMB damping scale measurements, there were already hints of high  $N_{\text{eff}}$  by combining the  $1+z_{\text{EQ}}$  constraint from *WMAP* with late-time observables sensitive to the matter density [25].

We now consider  $\rho_\Lambda$ . The angular scales of the acoustic peaks are highly sensitive to the angular size of the sound horizon,  $\theta_s = r_s/D_A$ . Thus,  $\theta_s$  is very precisely determined by the data. Given  $r_s$ , we could infer  $D_A$ . In a universe with zero mean spatial curvature,  $D_A = \int c dt/a$  from the time of last scattering to today, and depends only on  $\rho_m$  and  $\rho_\Lambda$ . We do know  $r_s$ , to some degree, from our determination of  $\rho_b$  and  $\rho_m$  as described above. These densities determine the history of the sound speed,  $c_s$  [59] and the expansion rate, allowing us to calculate  $r_s$  since it depends on no other parameters in the six-parameter  $\Lambda$ CDM model. This determination of  $r_s$  allows for a constraint on  $\rho_\Lambda$ .

### B. The Effect of Relativistic and Dark Degrees of Freedom

Changing  $N_{\text{eff}}$  only slightly alters the above story about the origins of the parameter constraints. We expect inferences of  $\rho_b$ ,  $1+z_{\text{EQ}}$  and  $\theta_s$  to be nearly unaffected. In the top panel of Fig. 1 we thus hold these parameters fixed while varying  $N_{\text{eff}}$  from 2 to 6. We hold  $z_{\text{EQ}}$  fixed by increasing the density of cold dark matter as we increase  $N_{\text{eff}}$ . We keep  $\theta_s$  fixed by changing  $\rho_\Lambda$  to adjust  $D_A$ .

As can be seen in Fig. 1, increasing  $N_{\text{eff}}$  along the chosen direction in parameter space, makes very little difference at low  $\ell$  (exactly as intended) and an increasing difference at higher  $\ell$ . A similar exercise was performed in [26], who identified the same parameters to be held fixed. They were interested in the region of the first three peaks and ascribed the relative drop in power toward the third peak as due to a post-decoupling effect known as the "early integrated Sachs-Wolfe effect.". We claim, in contrast, that the drop in power in the damping tail (beyond the second and third peaks) is almost entirely due to increased Silk damping, caused by the increased expansion rate. To demonstrate that the variation is not predominantly due to ISW, in the central panel we have normalized the spectra at  $\ell = 400$  where the ISW effect is negligible; we see that the high- $\ell$  variation is only slightly reduced.

Temperature anisotropies on scales smaller than the photon diffusion length are damped by the diffusion, a phenomenon known as Silk damping. Diffusion causes the drop in power toward high  $\ell$  and makes the power spectrum sensitive to the angular scale of the diffusion

length,  $\theta_d$ . To second order in  $\lambda_{\text{mfp}}/\lambda$ , where  $\lambda_{\text{mfp}}$  is the photon mean free path, the temperature fluctuations are suppressed by  $\exp[-(2r_d/\lambda)^2]$  where the mean squared diffusion distance at recombination is

$$r_d^2 = \pi^2 \int_0^{a_*} \frac{da}{a^3 \sigma_T n_e H} \left[ \frac{R^2 + \frac{16}{15}(1+R)}{6(1+R^2)} \right] \quad (1)$$

where  $n_e$  is the number density of free electrons,  $\sigma_T$  is the Thomson cross-section,  $a_*$  is the scale factor at recombination (defined below) and the factor in square brackets is due to the directional and polarization dependence of Thomson scattering [27, 28]. Although Eq. 1 is only an approximation to the diffusion length, it allows an analytic understanding of the dependence of this diffusion length on model parameters [20].

If we approximate  $a_*$  as independent of  $H$ , then  $r_d \propto H^{-0.5}$ . This is as expected for a random walk process: the distance increases as the square root of time. Increasing  $H$  (which happens when we increase  $N_{\text{eff}}$ ) leads to smaller  $r_d$  which would decrease the amount of damping. Why do we see, in Fig. 1, the damping increase as  $N_{\text{eff}}$  increases?

The answer has to do with how  $r_s$  and  $D_A$  change to keep  $\theta_s$  fixed despite the increased expansion rate. The comoving sound horizon is given by

$$r_s = \int_0^{t_*} c_s dt/a = \int_0^{a_*} \frac{c_s da}{a^2 H}. \quad (2)$$

Since  $r_s \propto 1/H$ , it responds even more rapidly to changes in  $H$  than is the case for  $r_d$ . To keep  $\theta_s$  fixed at the observed value,  $D_A$  must also scale as  $1/H$ . Since  $D_A$  decreases by more than would be necessary to keep  $\theta_d$  fixed,  $\theta_d$  increases which means the damping is increased.

To look at it another way, if we knew  $D_A$  perfectly, we could use  $r_s$  to determine  $H$  prior to recombination. But we do not know  $D_A$ , largely because we do not know the value of the cosmological constant, or more generally the density of the dark energy as a function of the scale factor. Instead, we can use the two scales together to form a ratio that is sensitive to  $H$ , with no dependence on  $D_A$ :  $\theta_d/\theta_s = r_d/r_s \propto H^{0.5}$ .

Does this explanation hold together quantitatively? To demonstrate that what we are seeing in the power spectrum actually is increased Silk damping (at fixed  $\theta_s$ ) we experiment with also fixing  $\theta_d$  as  $N_{\text{eff}}$  increases. The bottom panel of Fig. 1 shows how the angular power spectrum responds to the same variations in  $N_{\text{eff}}$ , only now taken at constant  $\theta_d$  as well. When we remove the  $\theta_d$  variation, the impact of the  $N_{\text{eff}}$  variation almost entirely disappears. We conclude that the variations we are seeing in the top panel are indeed due to the impact of  $N_{\text{eff}}$  on the amount of Silk damping. A very similar demonstration was provided by [21].

To keep  $\theta_d$  fixed as  $N_{\text{eff}}$  varies, we varied a parameter whose sole impact is on the number density of electrons: the primordial fraction of baryonic mass in Helium,  $Y_P$ . Even as early as times when 99% of the photons have yet

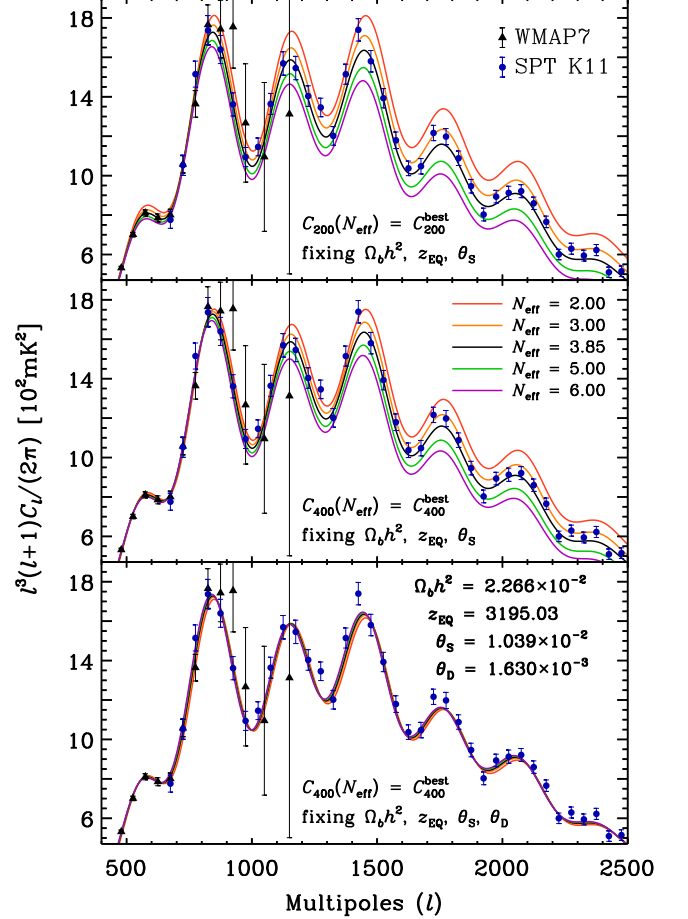


FIG. 1: *Top panel:* WMAP and SPT power spectrum measurements, and theoretical power spectra normalized at  $\ell = 200$ . The black (central) curve is for the best-fit  $\Lambda\text{CDM} + N_{\text{eff}}$  model assuming BBN consistency. The other model curves are for  $N_{\text{eff}}$  varying from 2 to 6 with  $\rho_b$ ,  $\theta_s$ , and  $z_{\text{EQ}}$  held fixed. Larger  $N_{\text{eff}}$  corresponds to lower power. *Central panel:* Same as above except normalized at  $\ell = 400$  where the ISW contribution is negligible. We see most of the variation remains. *Bottom panel:* The same as the central panel except we vary  $Y_P$  to keep  $\theta_d$  fixed. The lack of scatter in these spectra compared to those in the middle panel demonstrates that the effect of  $N_{\text{eff}}$  on small-scale data is largely captured by its impact on the damping scale. We can also begin to see more subtle effects of the neutrinos, most noticeably a phase shift in the acoustic oscillations [21].

to last scatter, Helium, with its greater binding energy than Hydrogen, is almost entirely neutral. Thus  $n_e = X_e(n_p + n_H) = X_e n_b(1 - Y_P)$  where the first equality defines  $X_e$  and we have kept  $n_b$  (and thus  $\rho_b$ ) fixed. The limit of integration in the above equations for  $r_s$  and  $r_d$  is only slightly affected by changing  $Y_P$  and thus  $r_s$  is largely unaffected. However, the damping length scales with  $Y_P$  as  $r_d \propto (1 - Y_P)^{-0.5}$ .

From our analysis one finds that  $r_d/r_s \propto (1 + f_\nu)^{0.25}/\sqrt{1 - Y_P}$  where  $f_\nu \equiv \rho_\nu/\rho_\gamma$  is proportional to

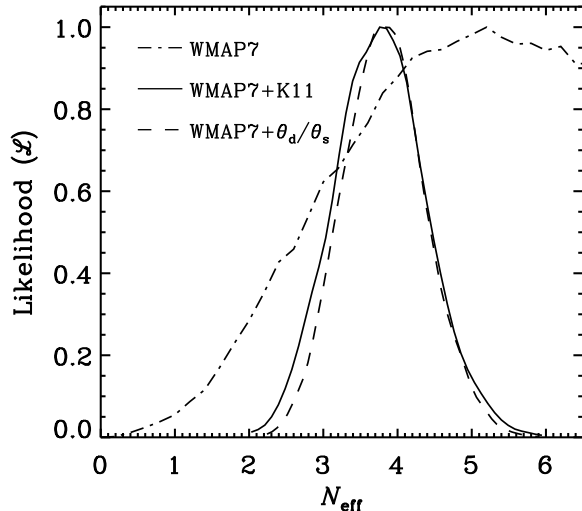


FIG. 2: Probability distribution of  $N_{\text{eff}}$  using just *WMAP* data, *WMAP* + SPT, and *WMAP* + constraints on  $\theta_d/\theta_s$  from *WMAP* + SPT (see Tab. I).

$N_{\text{eff}}$ . The first factor arises because increasing  $H$  at fixed  $z_{\text{EQ}}$  means  $H^2 \propto (1+f_\nu)$ . Thus as  $N_{\text{eff}}$  is varied, we know how to change  $Y_P$  to keep  $r_d/r_s$  (and hence  $\theta_d/\theta_s$ ) fixed.

However, the above analysis requires a small correction for two reasons. First, increased expansion, even if we keep  $n_e(a)$  fixed, decreases  $a_*$  because we define  $a_*$ , following [29], such that the optical depth to Thomson scattering from here to  $a_*$  is unity. Second, recombination is not a process that occurs in chemical equilibrium. As emphasized in [30], increasing the expansion rate leads to an increase in  $n_e(a)$ . By numerically studying these effects, which partially cancel each other, we find that  $r_d/r_s \propto (1+f_\nu)^m/\sqrt{1-Y_P}$  with  $m = 0.28$  rather than 0.25.

Note that when varying  $N_{\text{eff}}$  in Fig. 1, we also vary  $Y_P$  as is expected for standard assumptions about BBN, as will be explained below. Following BBN consistency (as opposed to keeping  $Y_P$  fixed) increases the damping effect by about 30%.

We should mention that neutrino perturbations do alter the amplitude of the power spectrum at  $l \gtrsim 200$  by a (nearly) constant factor [21, 31]. The breaking of the  $N_{\text{eff}}, \rho_m$  degeneracy in *WMAP* data at low  $N_{\text{eff}}$  is due to the impact of neutrino perturbations, and this is the effect that allowed for an indirect detection of these perturbations as reported in [32, 33].

However, with the inclusion of small-scale data, the perturbations have lost their significance. In Fig. 2 we demonstrate that the  $N_{\text{eff}}$  constraint from *WMAP* + SPT is well approximated by combining the *WMAP*7 data with the information on  $\theta_d/\theta_s$  from *WMAP* + SPT.

Fig. 3 provides another way of seeing the importance of  $\theta_d/\theta_s$  to the  $N_{\text{eff}}$  constraint. From the color coding one can see that lines of constant  $\theta_d/\theta_s$  run along the major axis of the probability contours. Further, one can

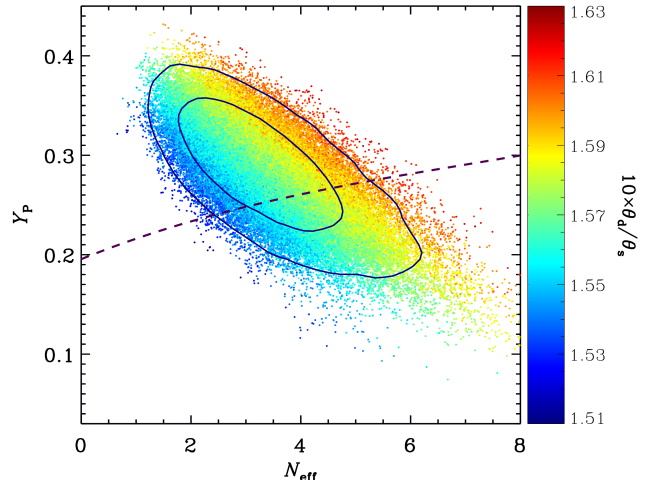


FIG. 3: The joint likelihood of  $N_{\text{eff}}$  and  $Y_P$  with 68% and 95% confidence contours. Each scattered point in the figure shows one element of the Markov chain with color coding the corresponding value of  $\theta_d/\theta_s$ . The purple dashed line is the BBN consistency line.

see that the BBN consistency line cuts nearly perpendicularly across these lines. This feature explains why the errors on  $N_{\text{eff}}$  are about 30% smaller if one assumes BBN consistency rather than fixed  $Y_P$ . If we abandon BBN consistency and allow  $Y_P$  to vary freely, then  $N_{\text{eff}}$  is allowed to vary along the major axis of the probability contours and the constraint on  $N_{\text{eff}}$  loosens considerably, as described in more detail below.

### C. Constraining $N_{\text{eff}}$ with $Y_P$ free

We do not have a complete analytic understanding of the closing of the contours on the major axis (as opposed to the minor axis) in Fig. 3. We can turn though to the lowest panel of Fig. 1 to see that at fixed  $\theta_d/\theta_s$  there is indeed some remaining variation to the power spectra as  $N_{\text{eff}}$  varies. At least some of this variation is due to the difference in acoustic oscillation phase shift that one gets for neutrinos, relative to the same energy density in photons, due to their free streaming [21].

Another effect important for breaking the degeneracy between  $Y_P$  and  $N_{\text{eff}}$  is due to high baryon fraction. In our above analysis we assumed that  $z_{\text{EQ}}$  is a fixed constant. However, this assumption will break down when  $N_{\text{eff}}$  decreases to lower values, as it can do if  $Y_P$  is allowed to vary freely, while the baryon density remains unchanged. As  $N_{\text{eff}}$  decreases, to keep  $z_{\text{EQ}}$  fixed,  $\omega_m$  would decrease, thus driving up the baryon fraction,  $\omega_b/\omega_m$ . Effects due to the high baryon fraction make it impossible at sufficiently low  $N_{\text{eff}}$  to find a value of  $z_{\text{EQ}}$ ,  $\omega_b$  and  $\omega_b/\omega_m$  that reproduce the measured power spectra. In an attempt to best accommodate the data, the region of

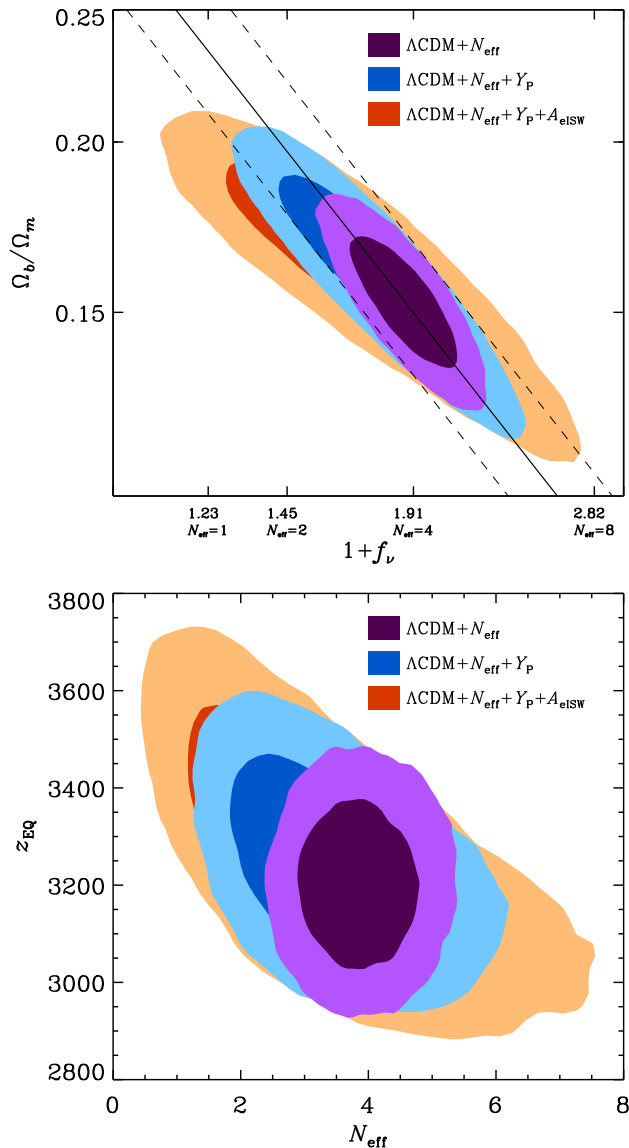


FIG. 4: Probability contours (68% and 95%) for the case of BBN consistency (purple), free  $Y_{\text{P}}$  (blue) and free  $Y_{\text{P}}$  and  $A_{\text{eISW}}$  (red). *Upper panel:* baryon fraction,  $\Omega_b/\Omega_m$  vs.  $(1+f_\nu)$ . The solid line is for  $100\Omega_b h^2 = 2.267$  and  $z_{\text{EQ}} = 3200$ . Varying  $z_{\text{EQ}}$  to 2843 (3557) we get the right (left) dashed line. One can see the constant  $z_{\text{EQ}}$  assumption breaks down at high baryon fraction. *Lower panel:* the  $N_{\text{eff}} - z_{\text{EQ}}$  plane. Here we can see more directly how the extra freedom degrades the inference of  $z_{\text{EQ}}$ .

high likelihood departs from constant  $z_{\text{EQ}}$ , as can be seen in the upper panel of Fig. 4 which shows probability contours in the  $(1+f_\nu) - \Omega_b/\Omega_m$  plane. The lines are lines of constant  $z_{\text{EQ}}$  and  $\omega_b$ . As extra freedom is allowed in the model, allowing  $N_{\text{eff}}$  to extend to lower values, we can see the expected departure of the probability ridge from the line of constant  $z_{\text{EQ}}$  and  $\omega_b$ , mainly due to variation of  $z_{\text{EQ}}$ .

A high baryon fraction alters the acoustic dynamics

for modes entering the horizon during matter domination, because a large fraction of the matter sourcing the gravitational potentials is feeling pressure support. This pressure support causes potentials to decay, boosting the amplitude of the fluctuations as happens with the “radiation driving” in the radiation-dominated era. At fixed  $\omega_b$ , increasing  $\omega_b/\omega_m$  boosts the height of the first peak relative to the second. The existence of this radiation-driving-like effect in the matter-dominated era impacts the ability to constrain  $z_{\text{EQ}}$ . One can see in the lower panel of Fig. 4 how the uncertainty in  $z_{\text{EQ}}$  increases when  $N_{\text{eff}}$  is allowed to take on smaller values (as happens when allowing  $Y_{\text{P}}$  to vary freely). The effect is even greater when allowing further freedom in the model by allowing  $A_{\text{eISW}}$  to vary, a parameter we will introduce below.

### III. CONSTRAINTS ON $N_{\text{eff}}$

Here we present constraints on  $N_{\text{eff}}$  from current data. We begin with our baseline estimates, which are from CMB data alone, assuming the six-parameter  $\Lambda\text{CDM}$  model extended by one to allow free  $N_{\text{eff}}$ , with  $Y_{\text{P}}$  determined by a BBN consistency relation to be discussed below.

We also consider departures from our baseline assumptions. We let  $Y_{\text{P}}$  vary away from the standard BBN relationship, let  $dn_s/d\ln k$  vary away from what is expected from inflation and allow the early ISW effect to be greater or smaller than expected, by introducing an phenomenological scaling parameter,  $A_{\text{eISW}}$ .

Finally, we consider the influence of low-redshift distance measurements on inferences of  $N_{\text{eff}}$ .

#### A. Baseline Constraints

We show our baseline constraints on  $N_{\text{eff}}$  in the first row of estimates of Table I, which is essentially the same with what Keisler et al. [4] have found for the same model.

#### B. Sensitivity to BBN Assumptions

The standard assumption is that the baryon-to-photon ratio and  $N_{\text{eff}}$  are unchanged from BBN through decoupling. However, many processes can change this situation, such as energy injection into the plasma after BBN which would reduce both  $\omega_b$  and  $N_{\text{eff}}$ , or a decay of a massive dark species into a relativistic dark species after BBN, which would increase  $N_{\text{eff}}$  while leaving  $\omega_b$  unchanged. Here we relax the standard assumption and distinguish the variables with superscripts DEC (for decoupling) and BBN.

First we consider the extreme of making no assumptions about BBN and using no light-element abundance data to constrain the BBN quantities. In practice this

TABLE I: Sensitivity of inferences of  $N_{\text{eff}}$  and  $\omega_b$  to BBN assumptions

Assumptions	Data	$100 \omega_b^{\text{BBN}}$	$100 \omega_b^{\text{DEC}}$	$100 \Delta \omega_b$	$N_{\text{eff}}^{\text{BBN}}$	$N_{\text{eff}}^{\text{DEC}}$	$\Delta N_{\text{eff}}$	$\omega_m$	$10 \theta_d / \theta_s$
Baseline	CMB	—	$2.27 \pm 0.05$	—	—	$3.86 \pm 0.62$	—	$0.148 \pm 0.012$	$1.569 \pm 0.015$
BBN $\neq$ DEC	CMB	—	$2.26 \pm 0.05$	—	—	$3.28^{+1.09}_{-0.89}$	—	$0.140^{+0.018}_{-0.015}$	$1.569 \pm 0.015$
BBN $\neq$ DEC	CMB+D/H+ $Y_P^A$	$2.29 \pm 0.11$	$2.26 \pm 0.06$	$-0.023^{+0.123}_{-0.127}$	$3.80 \pm 0.26$	$3.76^{+0.77}_{-0.73}$	$-0.033^{+0.829}_{-0.793}$	$0.147 \pm 0.014$	$1.567 \pm 0.015$
BBN $\neq$ DEC	CMB+D/H+ $Y_P^P$	$2.16^{+0.11}_{-0.10}$	$2.27 \pm 0.05$	$0.105^{+0.118}_{-0.124}$	$3.09 \pm 0.21$	$3.93^{+0.79}_{-0.75}$	$0.843^{+0.829}_{-0.794}$	$0.149^{+0.015}_{-0.014}$	$1.566 \pm 0.015$
$\omega_b^{\text{BBN}} = \omega_b^{\text{DEC}}$	CMB+D/H $^{\text{PC}}$	—	$2.27 \pm 0.05$	—	$3.31 \pm 0.58$	$3.93 \pm 0.74$	$0.617^{+0.896}_{-0.841}$	$0.149 \pm 0.014$	$1.567 \pm 0.015$

The PC superscript indicates the Pettini and Cooke (2012) inference, A indicates Aver et al. (2011) and P indicates Peimbert et al. (2007). The difference  $\Delta \omega_b \equiv \omega_b^{\text{DEC}} - \omega_b^{\text{BBN}}$ , and  $\Delta N_{\text{eff}} \equiv N_{\text{eff}}^{\text{DEC}} - N_{\text{eff}}^{\text{BBN}}$ .

simply means allowing  $Y_P$  to be free. As one would expect from our earlier discussion, allowing  $Y_P$  to be a free parameter greatly relaxes the constraints on  $N_{\text{eff}}^{\text{DEC}}$  because of its impact on  $\theta_d/\theta_s$ . This is shown in the second row of Table I.

If we assume standard BBN, we can use measurements of the abundance of Deuterium relative to Hydrogen,  $D/H$ , and  $Y_P$  to determine  $\omega_b^{\text{BBN}}$  and  $N_{\text{eff}}^{\text{BBN}}$ . Simha and Steigman [34] provided fitting formulae for the dependence of  $Y_P$  and  $D/H$  on these quantities. Here we present revised ones [60], that incorporate updates in nuclear reaction rate estimates and a neutron lifetime estimate. They are

$$Y_P = 0.2381 \pm 0.0006 + [\eta_{10} + 100(S - 1)] / 625 \quad (3)$$

and

$$10^5 D/H = 2.60(1 \pm 0.06) \left[ \frac{6}{\eta_{10} - 6(S - 1)} \right]^{1.6} \quad (4)$$

where

$$\begin{aligned} \eta_{10} &\equiv 10^{10} n_b / n_\gamma = 273.9 \omega_b + 100(S - 1) \quad \text{and} \\ S &= [1 + 7(N_{\text{eff}} - 3.046) / 43]^{1/2}. \end{aligned} \quad (5)$$

To calculate  $Y_P$  as a function of  $\omega_b$  and  $N_{\text{eff}}$  we use the default CosmoMC option which is an interpolation over tables produced using PARthENoPE v1.00 described in Pisanti et al. [35], only using Eq. 3 for values outside the bounds of the tables for robustness but very rarely reached. To calculate  $D/H$  we use Eq. 4.

For the measurements of light element abundances we mostly follow Nollett and Holder [36]. They assumed, from a compilation of  $D/H$  measurements (see Pettini et al. [37], Fumagalli et al. [38] and references therein)

$$\log(D/H) = -4.556 \pm 0.034. \quad (6)$$

We also consider a very recent, and significantly more precise,  $D/H$  measurement by Pettini and Cooke [39] of

$$\log(D/H) = -4.596 \pm 0.009. \quad (7)$$

Note that significant uncertainty arises from nuclear reaction rate uncertainty. When using  $D/H$  measurements we include the 6% error in Eq. 4 and add it in quadrature with the measurement error.

For Helium Nollett and Holder [36] considered two different inferences

$$\begin{aligned} Y_P &= 0.2573 \pm 0.0033 \quad (\text{Aver}) \\ Y_P &= 0.2477 \pm 0.0029 \quad (\text{Peimbert}) \end{aligned} \quad (8)$$

from Aver et al. [14] and Peimbert et al. [40] respectively; we will do the same.

Including the light element abundance measurements to help constrain  $Y_P$  reduces the uncertainty in  $N_{\text{eff}}^{\text{DEC}}$ , though it remains comparatively large. Interestingly, the lower  $Y_P$  measurement, which is the only one of the two consistent with  $N_{\text{eff}}^{\text{BBN}} = 3$ , leads to a slightly higher  $N_{\text{eff}}^{\text{DEC}}$  inference. This is because lower  $Y_P$  values need higher  $N_{\text{eff}}$  to get the same  $\theta_d/\theta_s$ .

Pettini and Cooke [39] took an inference of the baryon density from Keisler et al. [4], calculated assuming  $N_{\text{eff}} = 3.046$ , combined it with their  $D/H$  measurement, and the above  $D/H$  fitting formula, and found  $N_{\text{eff}}^{\text{BBN}} = 3.0 \pm 0.5$ . Thus they show that their data are consistent with the combination of CMB data and the assumption of  $N_{\text{eff}}^{\text{BBN}} = N_{\text{eff}}^{\text{DEC}} = 3.046$ .

We performed a similar, but different, exercise where we set  $\omega_b^{\text{DEC}} = \omega_b^{\text{BBN}}$  and estimated both  $N_{\text{eff}}$  values simultaneously from the CMB and  $D/H$  data. There is a small correlation between  $\omega_b$  and  $N_{\text{eff}}$  as inferred from the CMB data which leads to increased  $\omega_b$  inference when  $N_{\text{eff}}$  is allowed to vary. The net result is that our exercise leads to a higher value,  $N_{\text{eff}}^{\text{BBN}} = 3.3 \pm 0.6$ , with  $N_{\text{eff}}^{\text{DEC}} = 3.93 \pm 0.74$ .

We note that our analysis, in which we allow the BBN quantities to be different from the DEC quantities, is for a very general scenario and therefore missing features that may be important for specific scenarios. For example, in Eggers Bjaelde et al. [41] a scenario was considered in which  $N_{\text{eff}}$  increases after BBN due to the decay of a fraction of the dark matter into dark radiation. With such a specific choice, one can include in the calculation the details of how this conversion happens over time, and the differences in the dark radiation perturbations from the case of thermally produced neutrinos.



TABLE II: Sensitivity of inferences of  $N_{\text{eff}}$  to low-redshift distance measurements,  $dn_s/d \ln k$  and the phenomenological amplitude of the early ISW effect

Assumptions	Data	$100 \omega_b^{\text{DEC}}$	$N_{\text{eff}}^{\text{DEC}}$	$dn_s/d \ln k$	$A_{\text{eISW}}$	$\Omega_\Lambda$	$\omega_m$	$10 \theta_d/\theta_s$
Baseline	CMB	$2.27 \pm 0.05$	$3.86 \pm 0.62$	—	—	$0.737 \pm 0.025$	$0.148 \pm 0.012$	$1.569 \pm 0.015$
	CMB+BAO	$2.25 \pm 0.05$	$3.83 \pm 0.60$	—	—	$0.707 \pm 0.012$	$0.154 \pm 0.012$	$1.569 \pm 0.015$
	CMB+ $H_0$	$2.26 \pm 0.04$	$3.73 \pm 0.44$	—	—	$0.733 \pm 0.021$	$0.147 \pm 0.011$	$1.566 \pm 0.012$
	CMB+BAO+ $H_0$	$2.26 \pm 0.04$	$3.97 \pm 0.41$	—	—	$0.708 \pm 0.011$	$0.156^{+0.009}_{-0.008}$	$1.572 \pm 0.011$
$dn_s/d \ln k$ free	CMB	$2.21 \pm 0.07$	$2.97^{+0.91}_{-0.80}$	$-0.025 \pm 0.020$	—	$0.704 \pm 0.041$	$0.138^{+0.014}_{-0.012}$	$1.547^{+0.022}_{-0.021}$
$dn_s/d \ln k$ free	CMB+BAO+ $H_0$	$2.25 \pm 0.04$	$3.76 \pm 0.43$	$-0.015 \pm 0.013$	—	$0.706 \pm 0.011$	$0.153 \pm 0.009$	$1.566 \pm 0.012$
$A_{\text{eISW}}$ free	CMB	$2.29 \pm 0.08$	$3.92 \pm 0.65$	—	$0.979 \pm 0.055$	$0.741 \pm 0.028$	$0.149 \pm 0.012$	$1.568 \pm 0.015$
$A_{\text{eISW}}$ free	CMB+ $H_0$	$2.26 \pm 0.06$	$3.72 \pm 0.44$	—	$0.990 \pm 0.048$	$0.734 \pm 0.022$	$0.147 \pm 0.011$	$1.565 \pm 0.013$
$Y_P, A_{\text{eISW}}$ free	CMB	$2.24 \pm 0.11$	$3.07^{+1.59}_{-1.20}$	—	$1.011 \pm 0.076$	$0.726^{+0.035}_{-0.041}$	$0.137^{+0.024}_{-0.018}$	$1.569 \pm 0.015$

### C. Sensitivity to primordial power spectrum assumptions

Another straightforward way to reduce small-scale power is to alter the primordial power spectrum. For the usual power-law assumption, the exponent  $n_s$  is sufficiently well determined by low- $\ell$  data that it cannot mimic the damping effect of  $N_{\text{eff}}$ . However, if we allow for  $n_s$  to have a logarithmic scale dependence so that  $n_s(k) = n_s(k_*) + \ln(k/k_*) dn_s/d \ln k$  for some constant  $dn_s/d \ln k$  then the resulting power spectra can better mimic the effects of  $N_{\text{eff}}$ . As a result, if we marginalize over  $dn_s/d \ln k$ , we increase the uncertainty in  $N_{\text{eff}}$ , as can be seen in Table II.

### D. Importance of the early ISW Effect

The anisotropy field today can be written as an integration over perturbation variables on the past light cone. Doing so can be useful both computationally [42] and for analytic understanding. Writing the Fourier and Legendre-transformed radiation transfer function as such an integral (ignoring the polarization-dependence of Thomson scattering for simplicity) one gets

$$\begin{aligned}
 \Theta_l(k) = & \int_0^{\eta_0} d\eta g(\eta) [\Theta_0(k, \eta) + \Psi(k, \eta)] j_l[k(\eta_0 - \eta)] \\
 & - \int_0^{\eta_0} d\eta g(\eta) \frac{iv_b(k, \eta)}{k} \frac{d}{d\eta} j_l[k(\eta_0 - \eta)] \\
 & + \int_0^{\eta_0} d\eta f(z(\eta), A_{\text{eISW}}) e^{-\tau} [\dot{\Psi}(k, \eta) - \dot{\Phi}(k, \eta)] \\
 & \times j_l[k(\eta_0 - \eta)].
 \end{aligned} \quad (9)$$

See Dodelson [43] for definitions. The final integral is the so-called integrated Sachs-Wolfe (ISW) effect. The other terms are only important when the visibility function,  $g(\eta)$  is non-zero, whereas the ISW term gets contributions along the whole line of sight between here and recombination where  $\tau$  starts to get very large. The gravitational potential time derivatives are zero for a Universe dominated by cold dark matter. They are significantly non-zero at early times as the radiation density is still

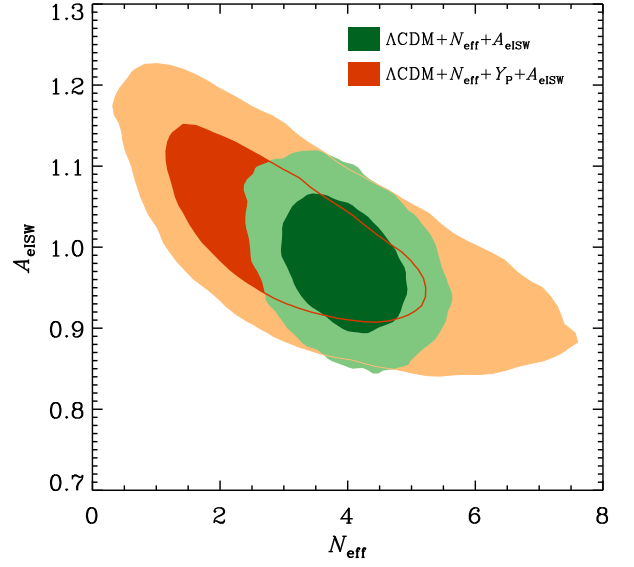


FIG. 5: Probability contours (68% and 95%) in the  $A_{\text{eISW}} - N_{\text{eff}}$  plane assuming BBN consistency (green, tighter contours) and free  $Y_P$  (red, broader contours). We see in the BBN-consistent case that the constraint on  $N_{\text{eff}}$  persists despite the freedom in the phenomenological amplitude of the early ISW effect. For the case of free  $Y_P$ ,  $A_{\text{eISW}}$  is important for constraining  $N_{\text{eff}}$ ; letting the amplitude vary freely degrades the constraints on  $N_{\text{eff}}$  somewhat, especially at low  $N_{\text{eff}}$ .

a significant contributor to the expansion rate (the early ISW effect), and then again at late times when dark energy becomes important (the late ISW effect).

In Eq. 9 we have introduced the parameter  $A_{\text{eISW}}$  so we can artificially vary the amplitude of the early ISW effect. The function  $f(z(\eta), A_{\text{eISW}}) = A_{\text{eISW}}$  when the redshift,  $z > 30$  and otherwise equals one. This use of  $A_{\text{eISW}}$  is very similar to the use of  $A_{\text{lens}}$  to artificially change the amplitude of the lensing potential power spectrum altering the CMB power spectrum. We might have chosen  $f$  to go as the square root of  $A_{\text{eISW}}$  so that  $A_{\text{eISW}}$  is scaling the ISW power (just as  $A_{\text{lens}}$  scales up the lensing power). However, a significant impact of the ISW term



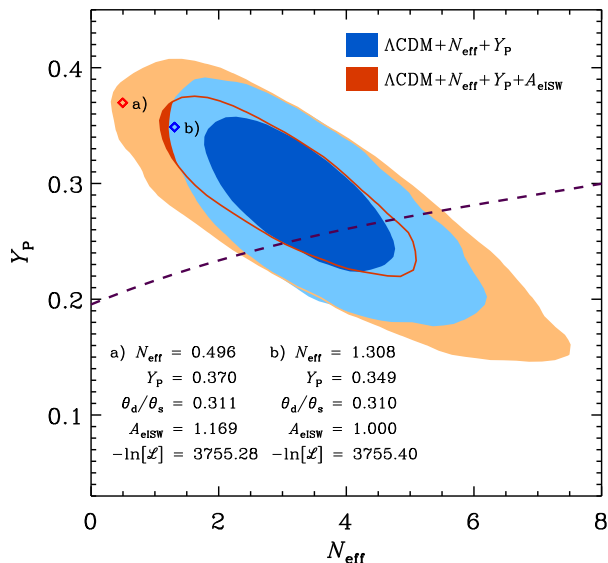


FIG. 6: Allowing  $A_{\text{eISW}}$  to vary stretches out the contours in the  $Y_P$  plane in the direction not constrained by  $\theta_d/\theta_s$ . If we assume BBN consistency though (the dashed line), then it has very little impact on the constraint on  $N_{\text{eff}}$ . Along the direction of constant  $\theta_d/\theta_s$ , two samples, a) and b), in the two Markov chains are picked up with almost identical likelihood values. The parameters of interest of these two samples are listed, and the corresponding power spectra are plotted in Fig. 7 with the  $A_{\text{eISW}}$  modulation turned off and on.

in Eq. 9 comes from its correlation with the other terms in the equation. Thus there is no way to make the total contribution of early ISW to the power scale as a single power of  $A_{\text{eISW}}$ .

The greater the amount of radiation around, relative to matter, at recombination, the greater the amplitude of the early ISW effect. Thus increasing  $N_{\text{eff}}$  (with  $\omega_m$  held fixed) would increase the amplitude of the early ISW effect. This relationship between  $N_{\text{eff}}$  and the early ISW effect led Bowen et al. [26] to cite the ISW effect as the reason the CMB is sensitive to  $N_{\text{eff}}$ .

To quantitatively investigate the impact of the ISW effect, we could perform the exercise of turning it off artificially. But turning off the ISW effect would so radically change the first peak (dropping it in power by 28%) that we instead chose to investigate by letting  $A_{\text{eISW}}$  be a free parameter. If the ISW effect is playing an important role in constraining  $N_{\text{eff}}$  then if we let it be a free parameter, those constraints will degrade and we will also see a strong correlation between the two parameters.

We show probability contours in the  $N_{\text{eff}}-A_{\text{eISW}}$  plane in Fig. 5 for the case that  $Y_P$  follows the BBN-consistency relation and the case that  $Y_P$  is free. For the BBN-consistent case, the constraint on  $N_{\text{eff}}$  degrades by less than 5% from  $N_{\text{eff}} = 3.86 \pm 0.62$  to  $N_{\text{eff}} = 3.92 \pm 0.65$ . The degradation on  $N_{\text{eff}}$  becomes negligible when the  $H_0$  prior is combined with CMB data as shown in Table II. This is consistent with what we have found in discussions

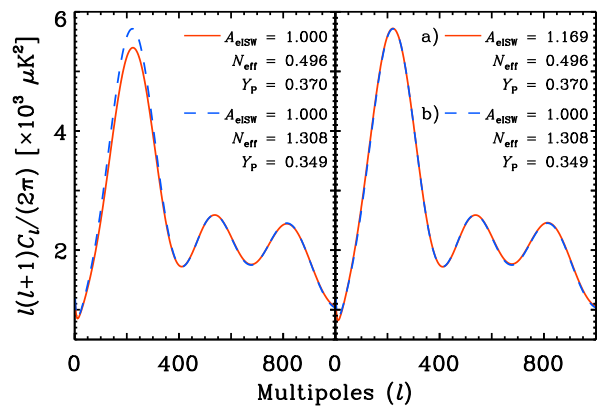


FIG. 7: The power spectra of the two samples shown in Fig. 6 with the  $A_{\text{eISW}}$  modulation turned off (on) in the left (right) panel. In this figure we see explicitly how allowing  $A_{\text{eISW}}$  to be artificially free weakens the lower bound on  $N_{\text{eff}}$  in the case that  $Y_P$  is free.

on Fig 2 that the constraint on  $N_{\text{eff}}$  is almost entirely due to the measurement of  $\theta_d/\theta_s$ .

However, when  $Y_P$  is allowed to vary freely, the  $\theta_d/\theta_s$  constraint can no longer determine  $N_{\text{eff}}$  because of the degeneracy with  $Y_P$ . In this case, the region of the spectrum affected by ISW is more important for determining  $N_{\text{eff}}$ . When  $A_{\text{eISW}}$  is also allowed to be free, it can modulate the height of the first acoustic peak and hence the baryon fraction, which leads to a wider range of  $Y_P$  variation due to its degeneracy with  $\omega_b$  during recombination and a wider  $N_{\text{eff}}$  constraint with fixed  $\theta_d/\theta_s$ . In Fig. 5, we do see a significantly enhanced degeneracy between  $A_{\text{eISW}}$  and  $N_{\text{eff}}$  when  $Y_P$  is allowed to be free. From Fig. 6 we can see that marginalizing over  $A_{\text{eISW}}$  does indeed loosen up the  $N_{\text{eff}}$ ,  $Y_P$  contour. The constraint on  $N_{\text{eff}}$  is degraded from  $N_{\text{eff}} = 3.28^{+1.09}_{-0.89}$  to  $N_{\text{eff}} = 3.07^{+1.59}_{-1.20}$  as shown in Table I and Table II. One can see explicitly in Fig. 7 how letting  $A_{\text{eISW}}$  vary allows lower  $N_{\text{eff}}$  and higher  $Y_P$  than would otherwise be possible.

We also see from Fig. 6 that marginalizing over  $A_{\text{eISW}}$  does little to expand the minor axis of the contours. As we have emphasized, the constraint along this axis is due to the constraint on  $\theta_d/\theta_s$ . Along the major axis the early ISW effect does play an important role in breaking the  $N_{\text{eff}} - Y_P$  degeneracy. Other effects important in breaking this degeneracy include those coming from neutrino perturbations [21] and high baryon fraction as discussed in Section II C.

#### IV. IMPLICATIONS FOR LOW-REDSHIFT DISTANCE MEASUREMENTS

We now consider the implications of CMB measurements, in the context of variable  $N_{\text{eff}}$ , for low-redshift measurements.

First let's consider the effect on the expansion rate at low redshift for the  $\Lambda\text{CDM} + N_{\text{eff}}$  cosmology. Increasing

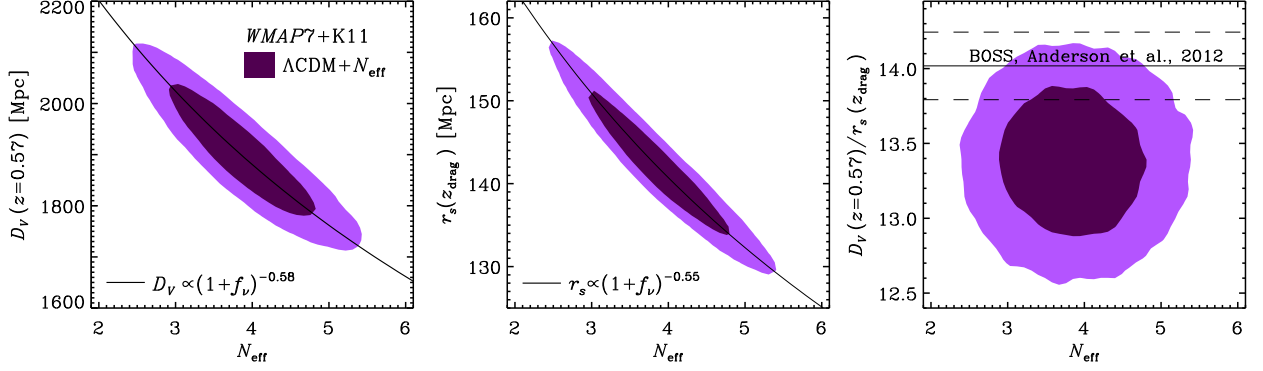


FIG. 8: *Left panel:* Contours of constant probability indicating the 68% and 95% confidence regions in the  $N_{\text{eff}} - D_V(z = 0.57)$  plane. The solid line shows the major correlation direction of  $D_V(z = 0.57) \propto (1 + f_\nu)^{-0.58}$  with the index best-fitted from the Markov chain. *Middle panel:* Probability contours in the  $N_{\text{eff}} - r_s(z_{\text{drag}})$  plane; the solid line holds the best-fit correlation direction  $r_s(z_{\text{drag}}) \propto (1 + f_\nu)^{-0.55}$ . *Right panel:* the relationship between  $N_{\text{eff}}$  and the ratio,  $D_V/r_s$ . The latest BOSS BAO data point [19] is plotted with the dashed line showing its  $1\sigma$  error, which is re-scaled by multiplying by the  $r_s$ -rescaling factor 154.66/150.82.

$N_{\text{eff}}$ , with the resulting increase in  $\omega_m \propto (1 + f_\nu)$  (to keep  $z_{\text{EQ}}$  fixed) increases the expansion rate through the matter-dominated era. Further, in order to adjust  $D_A$  to keep  $\theta_s$  fixed (given the decrease in  $r_s$ ), the energy density in the cosmological constant,  $\omega_\Lambda$ , must increase as well. With the energy density in both components important at low redshift increasing,  $H(z)$  increases for all redshifts in the low-redshift (matter-dominated and later) regime.

Note that if we can ignore changes to the limit of integration in Eq. 2 then we expect  $r_s(z_*) \propto (1 + f_\nu)^{-0.5}$ . With this scaling, we then expect  $D_A(z_*) \propto (1 + f_\nu)^{-0.5}$  to keep  $\theta_s$  fixed. The only way to achieve that scaling in the  $\Lambda$  CDM model is to have the dark energy density  $\omega_\Lambda$  scale in exactly the same way as  $\omega_m$ . Hence  $H(z)$ , and therefore  $D_A(z)$  scale the same way at all redshifts. If  $z_{\text{drag}}$  also has no variation with  $N_{\text{eff}}$  then the net result is that the BAO observables  $D_A(z)/r_s(z_{\text{drag}})$  and  $H(z) * r_s(z_{\text{drag}})$  have no dependence on  $N_{\text{eff}}$ . Note that  $z_{\text{drag}}$  is the epoch of photon-baryon decoupling defined as in Meiksin et al. [44].

In practice there are many corrections to the above analysis, e.g., the correlation between  $z_{\text{drag}}$  and  $N_{\text{eff}}$ , but they are all small and the net result is very little dependence of the BAO observables on  $N_{\text{eff}}$ . We can see that in Table II, where adding in just BAO data makes very little difference to the  $N_{\text{eff}}$  inference. Another consequence of  $\omega_\Lambda$  scaling similarly as  $\omega_m$  is that  $\Omega_\Lambda$  does not scale with  $N_{\text{eff}}$ .

Fig. 8 quantitatively supports the above discussion. We compute the quantity  $D_V \equiv (D_A^2 cz/H(z))^{1/3}$  at the redshift  $z = 0.57$  where the latest BAO data were effectively measured [19]. We see that  $D_V(z = 0.57) \propto (1 + f_\nu)^{-0.58}$ ,  $r_s(z_{\text{drag}}) \propto (1 + f_\nu)^{-0.55}$ ; i.e., they both scale nearly as  $(1 + f_\nu)^{-0.5}$ . And their scalings are

so similar that the ratio of the two quantities shows no noticeable correlation with  $N_{\text{eff}}$ . In the case of WMAP7+K11+BAO+ $H_0$ , we get  $\sigma(N_{\text{eff}}) = 0.41$ , compared to  $\sigma(N_{\text{eff}}) = 0.42$  in K11 [4] for our baseline model. The only difference comes from the latest BAO data point which shows a little tension with the  $D_V/r_s$  inference from the CMB data[61].

What is sensitive to  $N_{\text{eff}}$  at low redshift are absolute distance measures that are not calibrated with  $r_s$ . The inference of  $H_0$ , given  $\Lambda\text{CDM}$  (with standard radiation content) calibrated with the WMAP7 and SPT data is  $h = 0.710 \pm 0.021$ . This is  $1.17\text{-}\sigma$  lower than the Riess et al. 2011 value of  $h = 0.738 \pm 0.024$  [17]. Increasing  $N_{\text{eff}}$  to the higher value preferred by the CMB data alone brings these two inferences into better agreement. One can see the impact of the Riess et al. measurement on the reduced uncertainty in  $N_{\text{eff}}$  in the Table entries for the  $\Lambda\text{CDM} + N_{\text{eff}}$  cosmology; including the Riess et al. measurement drops the uncertainty by about 50%.

Varying  $N_{\text{eff}}$  thus changes the  $\Lambda\text{CDM}$ , CMB-calibrated predictions for  $H_0$ , without much change in the predictions for the BAO data – consistent with the analysis in Eisenstein and White [45]. Increasing  $N_{\text{eff}}$  thus can eliminate the tension between the BAO data and the Riess et al.  $H_0$  measurement as pointed out in Mehta et al. [18].

The case of  $dn_s/d\ln k$  free allows us to see this preference of the low-redshift data for the  $H(z)$  that comes from an increased  $N_{\text{eff}}$ . With CMB data alone, letting the running vary leads to a downward shift in the central value for  $N_{\text{eff}}$ . Adding in the  $H_0$  and BAO measurements shifts the preferred value for  $N_{\text{eff}}$  back up towards 4.

Increasing  $N_{\text{eff}}$  also has implications for the growth of structure. Increasing  $N_{\text{eff}}$  leads to an increase in  $\omega_m$  which in turn decreases  $\omega_b/\omega_m$ . Decreasing the baryon fraction decreases the pressure support felt by matter

prior to recombination, thereby boosting the growth of structure on scales smaller than the sound horizon at recombination; i.e., scales smaller than about 150 Mpc [46]. Therefore increasing  $N_{\text{eff}}$  increases cluster abundances, that are sensitive to the power spectrum amplitude on  $\sim 10$  Mpc scales. This effect can be seen in joint estimates of  $m_\nu$  (which has the opposite impact on small-scale power) and  $N_{\text{eff}}$  from cluster abundances in Benson et al. [47] and also in [48, 49].

## V. CONCLUSION

There are several ways that massless neutrinos impact the anisotropy of the cosmic microwave background. Here we have shown that current CMB constraints on  $N_{\text{eff}}$  are dominated by the impact of the neutrino energy density on the expansion rate. Although  $\theta_s$  is sensitive to this change in expansion rate from  $N_{\text{eff}}$ , its simultaneous sensitivity to the distance to last scattering greatly limits how well  $N_{\text{eff}}$  can be reconstructed from it alone. Measuring the damping tail region has allowed a measurement of  $\theta_d$  as well. Since the response of  $\theta_d$  to the expansion rate is different from the response of  $\theta_s$ , their ratio (which is independent of the distance to last scattering) is sensitive to the expansion rate.

The above analysis assumes that  $Y_P$  follows the BBN consistency relation. Since  $Y_P$  also alters  $\theta_d$ , allowing it to vary freely introduces a near degeneracy between  $N_{\text{eff}}$  and  $Y_P$ . This near degeneracy is broken by a number of physical effects at low  $N_{\text{eff}}$ , including the early ISW effect and effects of a high baryon fraction. At high  $N_{\text{eff}}$  the acoustic oscillation phase shifts probably play an important role, although we have not quantitatively confirmed this hypothesis.

We defined a phenomenological scaling parameter of the early ISW effect,  $A_{\text{eISW}}$ . We used it to study how much the early ISW effect plays a role in the  $N_{\text{eff}}$  constraint. After marginalizing over  $A_{\text{eISW}}$ , the constraint on  $N_{\text{eff}}$  degrades little for the BBN-consistent scenario. However, as just noted above, the early ISW effect does

contribute to constraints on  $N_{\text{eff}}$  when  $Y_P$  is allowed to vary freely. We found that, assuming BBN consistency,  $A_{\text{eISW}} = 0.979 \pm 0.055$  – a highly significant (though model dependent) detection of the early ISW effect.

We tested the consistency of inferences of  $\omega_b$ ,  $N_{\text{eff}}$  and  $Y_P$  from CMB data, with inferences from light element abundance measurements and BBN theory. We see no strong evidence for any inconsistency, though the bounds are quite loose. For the most discrepant case we find  $N_{\text{eff}}^{\text{DEC}} - N_{\text{eff}}^{\text{BBN}} = 0.84^{+0.83}_{-0.79}$ . We note that a simultaneous inference of  $N_{\text{eff}}^{\text{BBN}}$  and  $N_{\text{eff}}^{\text{DEC}}$  from the CMB and the new Pettini & Cooke D/H measurement results in an  $N_{\text{eff}}^{\text{BBN}}$  more consistent with 4 than is the case for the similar exercise performed in Pettini and Cooke [39].

We considered the impact of low-redshift distance-redshift relation measurements on determination of  $N_{\text{eff}}$ . We found that BAO data are not very sensitive to  $N_{\text{eff}}$  because  $D_V$  and  $r_s$  scale similarly with  $N_{\text{eff}}$ . The same cancellation does not occur for distance measures that calibrate independent of the CMB, such as the Hubble constant determination in Riess et al. [17].

We will have tighter measurements from the forthcoming analysis of the entire SPT survey, and we expect improvements to come from *Planck* in early 2013. We project that the error on  $N_{\text{eff}}$  will reduce to  $\sim 0.33$  using simulated full-survey SPT data combined with existing WMAP and  $H_0$  data, and will reduce further to  $\sim 0.20$  using simulated *Planck* data and existing  $H_0$  data, assuming the *Planck* data and foreground model of Millea et al. [50], consistent with the forecasts of Bashinsky and Seljak [21] and Hannestad et al. [51].

## Acknowledgments

We thank A. Albrecht, B. Benson, O. Doré, E. Komatsu, M. Luty, J. Ruhl, L. Strigari, A. Vikhlinin and M. White for useful conversations. We acknowledge support from NSF awards no. 0709498 and ANT-0638937. We used CosmoMC [52].

- 
- [1] C. L. Reichardt, P. A. R. Ade, J. J. Bock, J. R. Bond, J. A. Brevik, C. R. Contaldi, M. D. Daub, J. T. Dempsey, J. H. Goldstein, W. L. Holzapfel, et al., *Astrophys. J.* **694**, 1200 (2009), 0801.1491.
  - [2] S. Das, T. A. Marriage, P. A. R. Ade, P. Aguirre, M. Amiri, J. W. Appel, L. F. Barrientos, E. S. Battistelli, J. R. Bond, B. Brown, et al., *Astrophys. J.* **729**, 62 (2011), 1009.0847.
  - [3] J. Dunkley, R. Hlozek, J. Sievers, V. Acquaviva, P. A. R. Ade, P. Aguirre, M. Amiri, J. W. Appel, L. F. Barrientos, E. S. Battistelli, et al., *ArXiv:1009.0866* (2010), 1009.0866.
  - [4] R. Keisler, C. L. Reichardt, K. A. Aird, B. A. Benson, L. E. Bleem, J. E. Carlstrom, C. L. Chang, H. M. Cho, T. M. Crawford, A. T. Crites, et al., *Astrophys. J.* **743**, 28 (2011), 1105.3182.
  - [5] P. C. de Holanda and A. Y. Smirnov, *ArXiv:1012.5627* (2010), 1012.5627.
  - [6] W. Fischler and J. Meyers, *Phys. Rev. D* **83**, 063520 (2011), 1011.3501.
  - [7] L. M. Krauss, C. Lunardini, and C. Smith, *ArXiv:1009.4666* (2010), 1009.4666.
  - [8] S. Galli, M. Martinelli, A. Melchiorri, L. Pagano, B. D. Sherwin, and D. N. Spergel, *Phys. Rev. D* **82**, 123504 (2010), 1005.3808.
  - [9] K. Nakayama, F. Takahashi, and T. T. Yanagida, *Physics Letters B* **697**, 275 (2011), 1010.5693.
  - [10] S. Hannestad, A. Mirizzi, G. G. Raffelt, and Y. Y. Y. Wong, *JCAP* **8**, 1 (2010), 1004.0695.
  - [11] W. Fischler and W. T. Garcia, *Journal of High Energy*

- Physics **6**, 46 (2011), 1104.2078.
- [12] Y. I. Izotov and T. X. Thuan, *Astrophys. J. Lett.* **710**, L67 (2010), 1001.4440.
  - [13] E. Aver, K. A. Olive, and E. D. Skillman, *JCAP* **5**, 3 (2010), 1001.5218.
  - [14] E. Aver, K. A. Olive, and E. D. Skillman, *JCAP* **3**, 43 (2011), 1012.2385.
  - [15] A. A. Aguilar-Arevalo, C. E. Anderson, S. J. Brice, B. C. Brown, L. Bugel, J. M. Conrad, R. Dharmapalan, Z. Djurcic, B. T. Fleming, R. Ford, et al., *Physical Review Letters* **105**, 181801 (2010).
  - [16] G. Mention, M. Fechner, T. Lasserre, T. A. Mueller, D. Lhuillier, M. Cribier, and A. Letourneau, *ArXiv:1101.2755* (2011), 1101.2755.
  - [17] A. G. Riess, L. Macri, S. Casertano, H. Lampeitl, H. C. Ferguson, A. V. Filippenko, S. W. Jha, W. Li, and R. Chornock, *Astrophys. J.* **730**, 119 (2011), 1103.2976.
  - [18] K. T. Mehta, A. J. Cuesta, X. Xu, D. J. Eisenstein, and N. Padmanabhan, *ArXiv e-prints* (2012), 1202.0092.
  - [19] L. Anderson, E. Aubourg, S. Bailey, D. Bizyaev, M. Blanton, A. S. Bolton, J. Brinkmann, J. R. Brownstein, A. Burden, A. J. Cuesta, et al., *ArXiv e-prints* (2012), 1203.6594.
  - [20] W. Hu and M. White, *Astrophys. J.* **471**, 30 (1996), *arXiv:astro-ph/9602019*.
  - [21] S. Bashinsky and U. Seljak, *Phys. Rev. D* **69**, 083002 (2004), *arXiv:astro-ph/0310198*.
  - [22] W. Hu and S. Dodelson, *Annu. Rev. Astron. Astrophys.* **40**, 171 (2002), *arXiv:astro-ph/0110414*.
  - [23] W. Hu, M. Fukugita, M. Zaldarriaga, and M. Tegmark, *Astrophys. J.* **549**, 669 (2001), *arXiv:astro-ph/0006436*.
  - [24] J. C. Mather, E. S. Cheng, R. E. Eplee, Jr., R. B. Isaacman, S. S. Meyer, R. A. Shafer, R. Weiss, E. L. Wright, C. L. Bennett, N. W. Boggess, et al., *Astrophys. J. Lett.* **354**, L37 (1990).
  - [25] E. Komatsu, J. Dunkley, M. R. Nolte, C. L. Bennett, B. Gold, G. Hinshaw, N. Jarosik, D. Larson, M. Limon, L. Page, et al., *Astrophys. J. Supp.* **180**, 330 (2009), 0803.0547.
  - [26] R. Bowen, S. H. Hansen, A. Melchiorri, J. Silk, and R. Trotta, *Mon.Not.Roy.As.Soc.* **334**, 760 (2002), *arXiv:astro-ph/0110636*.
  - [27] N. Kaiser, *Mon.Not.Roy.As.Soc.* **202**, 1169 (1983).
  - [28] M. Zaldarriaga and D. D. Harari, *Phys. Rev. D* **52**, 3276 (1995), *arXiv:astro-ph/9504085*.
  - [29] W. Hu and N. Sugiyama, *Astrophys. J.* **444**, 489 (1995), *arXiv:astro-ph/9407093*.
  - [30] O. Zahn and M. Zaldarriaga, *Phys. Rev. D* **67**, 063002 (2003), *arXiv:astro-ph/0212360*.
  - [31] W. Hu, D. Scott, N. Sugiyama, and M. White, *Phys. Rev. D* **52**, 5498 (1995), *arXiv:astro-ph/9505043*.
  - [32] R. Trotta and A. Melchiorri, *Physical Review Letters* **95**, 011305 (2005), *arXiv:astro-ph/0412066*.
  - [33] F. De Bernardis, L. Pagano, P. Serra, A. Melchiorri, and A. Cooray, *JCAP* **6**, 13 (2008), 0804.1925.
  - [34] V. Simha and G. Steigman, *JCAP* **6**, 16 (2008), 0803.3465.
  - [35] O. Pisanti, A. Cirillo, S. Esposito, F. Iocco, G. Mangano, G. Miele, and P. D. Serpico, *Computer Physics Communications* **178**, 956 (2008), 0705.0290.
  - [36] K. M. Nollett and G. P. Holder, *ArXiv e-prints* (2011), 1112.2683.
  - [37] M. Pettini, B. J. Zych, M. T. Murphy, A. Lewis, and C. C. Steidel, *Mon.Not.Roy.As.Soc.* **391**, 1499 (2008), 0805.0594.
  - [38] M. Fumagalli, J. M. O'Meara, and J. X. Prochaska, *Science* **334**, 1245 (2011), 1111.2334.
  - [39] M. Pettini and R. Cooke, *ArXiv e-prints* (2012), 1205.3785.
  - [40] M. Peimbert, V. Luridiana, and A. Peimbert, *Astrophys. J.* **666**, 636 (2007), *arXiv:astro-ph/0701580*.
  - [41] O. Eggers Bjaelde, S. Das, and A. Moss, *ArXiv e-prints* (2012), 1205.0553.
  - [42] U. Seljak and M. Zaldarriaga, *Astrophys. J.* **469**, 437 (1996), *arXiv:astro-ph/9603033*.
  - [43] S. Dodelson, *Modern Cosmology* (Academic Press, Elsevier Science, 2003).
  - [44] A. Meiksin, M. White, and J. A. Peacock, *Mon.Not.Roy.As.Soc.* **304**, 851 (1999), *arXiv:astro-ph/9812214*.
  - [45] D. Eisenstein and M. White, *Phys. Rev. D* **70**, 103523 (2004), *arXiv:astro-ph/0407539*.
  - [46] D. J. Eisenstein and W. Hu, *Astrophys. J.* **496**, 605 (1998), *arXiv:astro-ph/9709112*.
  - [47] B. A. Benson, T. de Haan, J. P. Dudley, C. L. Reichardt, K. A. Aird, K. Andersson, R. Armstrong, M. Bautz, M. Bayliss, G. Bazin, et al., *ArXiv e-prints* (2011), 1112.5435.
  - [48] J. Hamann, S. Hannestad, G. G. Raffelt, I. Tamborra, and Y. Y. Y. Wong, *Physical Review Letters* **105**, 181301 (2010).
  - [49] J. Hamann, S. Hannestad, G. G. Raffelt, and Y. Y. Y. Wong, *JCAP* **9**, 34 (2011), 1108.4136.
  - [50] M. Millea, O. Doré, J. Dudley, G. Holder, L. Knox, L. Shaw, Y. Song, and O. Zahn, *ArXiv:1102.5195* (2011), 1102.5195.
  - [51] S. Hannestad, H. Tu, and Y. Y. Wong, *JCAP* **6**, 25 (2006), *arXiv:astro-ph/0603019*.
  - [52] A. Lewis and S. Bridle, *Phys. Rev. D* **66**, 103511 (2002), *arXiv:astro-ph/0205436*.
  - [53] D. Jungman, M. Kamionkowski, A. Kosowsky, and G. N. Spergel, *Physical Review Letters* **76**, 1007 (1996), *arXiv:astro-ph/9507080*.
  - [54] Jungman et al. [53] first pointed out that the number of species of relativistic neutrinos could be measured from CMB.
  - [55] The effective number of neutrinos is defined so that the neutrino and photon energy densities are related by  $\rho_\nu = N_{\text{eff}} \frac{7}{8} \left(\frac{4}{11}\right)^{4/3} \rho_\gamma$ .
  - [56] An exception is the breaking of the  $Y_P - N_{\text{eff}}$  degeneracy, to be discussed later.
  - [57] Energy densities today are often expressed as, e.g.,  $\Omega_b h^2 = \rho_b / (1.879 \times 10^{-29} \text{g/cm}^3)$
  - [58]  $\Omega_m \equiv 8\pi G \rho_m / (3H_0^2)$ .
  - [59]  $c_s^2 = \partial P / \partial \rho = 1/[3(1+R)]$  with  $R = 3\rho_b(z)/(4\rho_\gamma(z))$
  - [60] G. Steigman, private communication
  - [61] Note that Anderson et al. [19] report  $D_V/r_s$  for an  $r_s$  given by the fitting formula of Eisenstein and Hu [46]. We have adjusted the reported value for comparison to  $D_V/r_s$  calculated with our definition of  $r_s$  by multiplying it by 154.66/150.82. See [18]